CALCULATION OF MULTIBLADED ROTORS IN HIGH-SPEED FORWARD FLIGHT WITH WEAK FLUID-STRUCTURE-COUPLING

Klausdieter Pahlke
DLR, Institute of Aerodynamics and Fluid Technology
D-38108 Braunschweig, Lilienthalplatz 7
email: Klausdieter.Pahlke@dlr.de

Berend van der Wall
DLR, Institute of Flight Research
D-38108 Braunschweig, Lilienthalplatz 7
email: Berend.vanderWall@dlr.de

Summary: A weak coupling procedure for coupling the DLR rotor simulation code S4 and the DLR Euler/Navier-Stokes solver FLOWer is presented. The method allows to produce trimmed CFD solutions for rotors in high speed forward flight with inclusion of elastic blade deformations and viscous effects. The weak coupling procedure is applied to high-speed forward flight test cases of the 7A and the 7AD rotor. Isolated blade computations are carried out for both rotors while the full 4-bladed rotor is simulated only in the 7A case using the chimera approach. The predicted pitching moment computed with the assumption of inviscid flow (Euler solutions) shows large differences compared to the experimental data while viscous (Navier-Stokes) computations are in much better agreement with the measured data. The weak coupling considerably improved the solution compared to the uncoupled CFD computations. The performance difference between the 7A and the 7AD rotor in high-speed forward flight was fairly well predicted.

Nomenclature:

a_∞	free stream speed of sound
c	local blade chord
$C_m M^2$	local pitching moment coefficient $(P/(0.5\rho_\infty a_\infty^2 c^2 \text{ unit length}))$
$C_n M^2$	local normal force coefficient $(N/(0.5\rho_\infty a_\infty^2 c \text{ unit length}))$
M	local reference Mach number
M_∞	free stream Mach number
$M_{\omega R}$	Mach number due to rotational motion of the blade tip ($\omega R/a_\infty$)
N	normal force [N]
P	pitching moment [Nm]
r	radial coordinate [m]
R	rotor radius [m]
$y+$	non-dimensional distance normal to the blade surface
α_q	rotor shaft angle [^{o}]
β	flapping angle [^{o}]
μ	advance ratio ($M_\infty/M_{\omega R}$)
ϑ	elastic torsion angle [^{o}]
θ	pitch angle [^{o}], $\theta=\theta_0+\theta_S\sin(\psi)+\theta_C\cos(\psi)$
θ_0	collective pitch angle [^{o}]
θ_C	lateral pitch angle [^{o}]
θ_S	longitudinal pitch angle [^{o}]
ψ	azimuth angle [^{o}]
ω	rotational angular velocity [1/s]

1 Motivation

The main interest in applying CFD methods to aircraft configurations lies in the large potential of these methods for aircraft design. This requires the capability to predict forces and moments within certain error bands. In fact, acceptance criteria for a CFD method may not be extremely strict on absolute forces or moments. It is more important to prove that the method is able to assess different shapes with the correct trends and to correctly predict the aerodynamic improvements because of geometry variations.

The comparison of two helicopter rotors requires identical flight conditions (same lift and propulsive force and the same time averaged global pitching and rolling moment in the inertial system), if a reliable evaluation of the aerodynamic rotor performance is required. A prerequisite for this is a procedure that allows to compute trimmed CFD solutions with a realistic blade motion. Therefore, a method accounting for elastic blades with a coupling of aerodynamics and blade dynamics and with trim capability is required.

This task could be tackled with a method in which the aerodynamic forces and the blade dynamic motion are strongly coupled (i.e. the aerodynamic, inertial and elastic forces are balanced from time step to time step). In a strongly coupled computation 5-10 revolutions can be assumed to achieve a periodic solution for a given setting of rotor controls which highly depends on the damping of the various rotor blade degrees of freedom, especially in lead-lag and torsion. It should be noted that the blade motion is not known a priori but a result of the CFD computa-

tion. 10 trim steps might be necessary for a trimmed state, resulting in 50-100 rotor revolutions with a time marching solution scheme which have to be computed with an expensive CFD method like an Euler/Navier-Stokes solver. The idea behind the weak (or off-line) coupling is, that only a few (3-5) coupling iterations of the rotor simulation code with the expensive CFD method are required and that the CFD method will need only about 2 revolutions to get a periodic solution for each blade motion which is prescribed by the rotor simulation code. This results in 6-10 revolutions which have to be computed with the CFD method. Compared to the strong coupling this could save 90% of the computational effort. However, it has to be proven that the accuracy of the weak coupling approach is sufficient for assessing a given rotor design.

A brief overview on CFD methods for rotor aerodynamics is given in [1]. For an overview of the state of the art of coupling procedures for CFD methods for helicopter rotors and rotor aeromechanics codes please see [2]. All results presented in this paper have been achieved within the French-German cooperation CHANCE (Complete Helicopter Advanced Computational Environment) [3], [4].

2 Solution Algorithm

2.1 CFD Solver FLOWer

All computations of this paper have been computed with a modified version of the block-structured DLR flow solver FLOWer [6] (Release 116.5). FLOWer is a portable software system and can be run on a large variety of computers with high efficiency. It solves the unsteady Reynolds averaged Navier-Stokes equations, transformed into a moving blade fixed coordinate system. Details of the algorithm are given in [5]. The discretization of space and time is separated following the method of lines [7] using a cell-vertex finite volume formulation for the spatial discretization. In order to avoid spurious oscillations, a blend of first and third order dissipative terms is introduced. Two layers of auxiliary points are used to store the neighbour flow values in order to match the solutions across inner and external cuts with second order accuracy. In the code, different turbulence models are available. In the present work only the algebraic Baldwin-Lomax model [8] with the modification of Degani and Schiff [9] is applied. The time integration uses the dual time stepping technique with a second order implicit time integration operator [10]. An important speed-up of the computations is achieved by the multigrid technique. In order to allow for elastic blade motions deforming grids are used. Free stream consistency for deforming grids is guaranteed by a geometrical conservation

law [11]. At each time step the deformed blade surface is computed using a Fourier series for each of the blade mode shapes which was calculated with the rotor simulation code S4. The deformed volume grid is then generated using transfinite interpolation techniques. The method is independent of the block topology and can also be applied to multi-block cases. The grid quality close to the blade is of the same quality as the undeformed grid. For highly distorted grids the quality of the grid at inner cuts may be only fair.

2.2 Rotor Simulation Code S4

The DLR rotor code S4 originally was developed to compute effects of Higher Harmonic Control (HHC) onto dynamic rotor forces of a hingeless rotor in the nonrotating frame [14], [15]. With time, it evolved into a comprehensive code for the computation of isolated rotors with high resolution blade loads for acoustic postprocessing. It is validated by studies about active control of HHC or Individual Blade Control (IBC) [16], and the effects of dynamic stall[17]. It mainly consists of 3 modules:
The aerodynamics, the structural dynamics and the induced velocities module. They are embedded in a trim algorithm and comprise:
a)The aerodynamic module [18]-[20], with nonlinear unsteady aerodynamics (incl. Mach effects, dynamic stall, varying velocity effects and yaw influence). The blade is discretized into 20 elements of decreasing size radially. In each of them, the time histories of Mach numbers at the collocation point (located at three-quarter chord) are computed, which form the basis input of the unsteady aerodynamics computation. The local forces and moments are summed up into the generalized modal forces of the respective blade modes.
b)The structural dynamics module represents an arbitrary number of articulated or hingeless elastic blades. Each blade is represented by its mode shapes and natural frequencies in flap, lead-lag and torsion separately. Both the mode shapes and the natural frequencies are taken from either experiments or - usually- from a finite element computation. Within the rotor code, the generalized coordinates of each mode are computed by time integration of their differential equations of motion, having the generalized aerodynamic forcing (see above) on the right hand side of the equations. For this purpose, a Runge-Kutta 4th order scheme is used.
c)The third important module is associated with the induced velocities. For this study, a prescribed tip vortex wake [21] is used, together with rotor-body interactions and wind tunnel-body interactions [22].
The overall handling is done with an automatic trim module for specified non-rotating hub forces and moments. As degrees of freedom to trim to the desired values, the collective and cyclic controls are

used; and in addition the rotor shaft angle of attack is taken. The rotor trim is defined by measured values of vertical and propulsive forces, plus pitch and roll moment, and the wind tunnel data like temperature, pressure, and velocity.

3 Coupling Procedure for Weak Coupling

The coupling between the CFD method FLOWer and the rotor simulation code S4 is carried out as follows (see Figure 1). First a trim computation is carried out with S4 alone. After this trim computation the elastic blade motion based on the aerodynamic forces of the blade element theory is known. The CFD code is then applied with this prescribed blade motion including an elastic motion of the blade and provides a field of aerodynamic forces and moments for each blade element and each azimuth position.
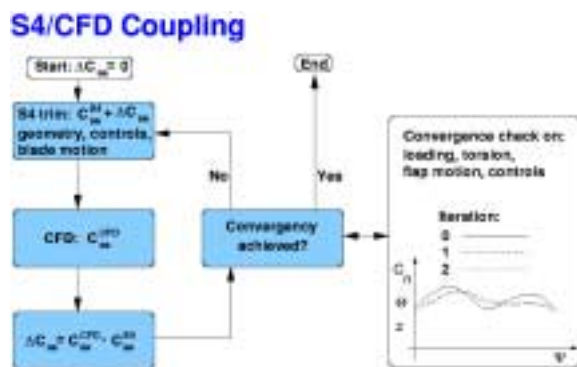
Figure 1   Block diagramm of coupling procedure
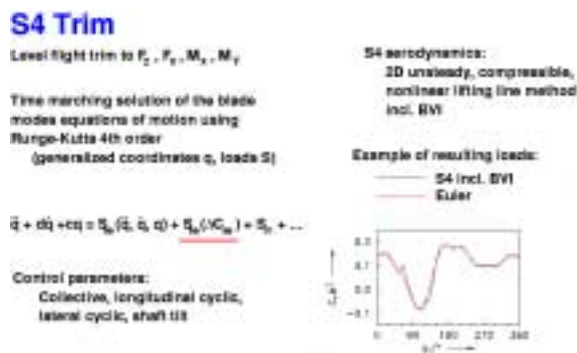
Figure 2   Trim procedure of the S4 rotor simulation code

The difference between the CFD aerodynamics and the S4 aerodynamics is computed. This difference is added to the S4 aerodynamic model in terms of normal forces $c_n M^2$ or normal forces *and* moments ($c_n M^2$ and $c_m M^2$) for the next iteration (see Figure 1). The new trim is now obtained based on the S4 aerodynamics plus the difference to the CFD aerodynamics. This procedure is repeated until the blade motion (control angles, rotor shaft angle and elastic blade motion) between two consecutive iterations is below a certain threshold. The lead-lag motion was neglected for the computations of this paper because

it is aerodynamically not very efficient although it may have important effects on the coupling of the flapping and torsion motion. In future applications the lead-lag motion will be considered as well as the tangential forces.

By this coupling method the equation of motion of the rotor blade is solved with the aerodynamic forces computed with the CFD method if the iteration process converges. In the isolated blade computations the blade wake can only be computed inside the CFD grid. When complete rotors are computed (even with the chimera method), the individual vortices are diffused due to numerical dissipation as a consequence of the coarseness of the CFD grids some chords away from the blade. This problem is associated with a loss of blade-vortex interaction (BVI) effects, and is overcome by the following procedure: The CFD results contain harmonics usually up to 6/rev, with rather small amplitudes in the frequencies above 6/rev.Therefore the CFD results are low-pass filtered at 6/rev, and the same is done with the S4 loads, which do include BVI due to the prescribed wake used. An aerodynamic difference matrix is computed for this low frequency content (e.g. $\Delta C_n M^2 = C_n M^2(\text{CFD}) - C_n M^2(\text{S4})$) and added to the next S4 trim as a non-variable aerodynamic offset. Thus, after convergence is obtained, the first 6 harmonics represent exactly the CFD aerodynamics, and all higher harmonics include BVI effects from S4, which are not contained in the CFD results.

4 Test Cases

High speed forward flight test cases of the fully articulated 4-bladed ONERA 7A and 7AD rotors were selected. The 7A and the 7AD rotors are fully instrumented rotors which were designed by ECF and tested in the ONERA S1 wind tunnel at the Modane test center (see [23]). The 7A rotor has rectangular blades whereas the 7AD rotor has a parabolic swept back tip with anhedral and a straight trailing edge. Both rotors have an aspect ratio of R/c=15. The test cases chosen correspond to a rotational tip speed Mach number of $M_{\omega R}=0.64$ with an advance ratio of $\mu=0.4$. Chordwise pressure distributions were measured at 5 spanwise stations (0.5R, 0.7R, 0.825R, 0.915R, 0.975R). The integration of these pressures is used to compute the experimental normal force coefficients and pitching moments at these stations.

5 Grid Generation

Grids were generated for two different approaches: single block grids around isolated blades and multiblock chimera grids around the whole 7A rotor.

An isolated blade computation means that only the near wake is part of the solution. The downwash of the other blades is not accounted for. This simplifi-

cation was done in order to reduce the computational effort, knowing that this will reduce the accuracy of the solution. As the selected test case is a high speed forward flight case, an acceptable agreement of the computational results close to the blade tip with the experimental data can be expected, because the effect of the induced velocities is comparably small at the blade tip for such high speed cases (except where BVI occurs). The vortical wake system is part of the solution in the case of the chimera computation.

The grids are of CH type and were generated as follows. First a set of 2d grids around each blade section was generated using an algebraic grid generator. This set was staggered to form a 3d grid which was 3d elliptically smoothed [12], [13]. If necessary, a boundary layer grid was splined into the 3d grid. The first spacing was set to 1.5e-5 which corresponds to y^+-values of about 1 for a Reynolds number of about 2e+6. The grid around the 7A rotor blade in the rotor plane is shown in Figure 3 while the grid at r/R=0.9 is presented in Figure 4. In Figure 5 the grid in the rotor plane of the 7AD rotor is plotted. Please note the parabolic swept back tip of the 7AD rotor. The grids around isolated blades have a farfield distance of 20 chords referred to the chord length at the blade root (r/R=0.2).
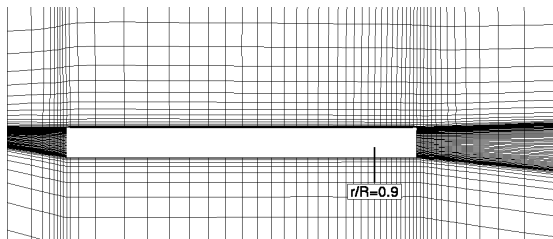
Figure 3   Isolated blade grid in rotor plane (7A rotor)
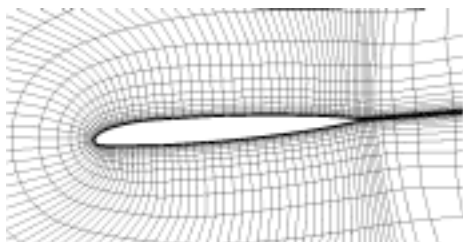
Figure 4   Grid section at r/R=0.9
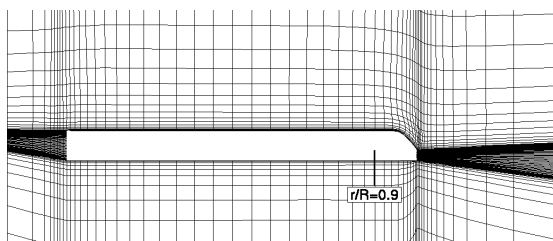
Figure 5   Isolated blade grid in rotor plane (7AD rotor)

The child grids for the chimera grid system around the 7A rotor were generated in the same manner as the grids around isolated blades except that the dis-

tance from the blade surface to the outer boundary of the child grids is about 3c. The farfield distance is at minimum 1R in all directions. A cartesian background grid with non-aequidistant spacing was used (see Figure 6, only every other grid point printed).
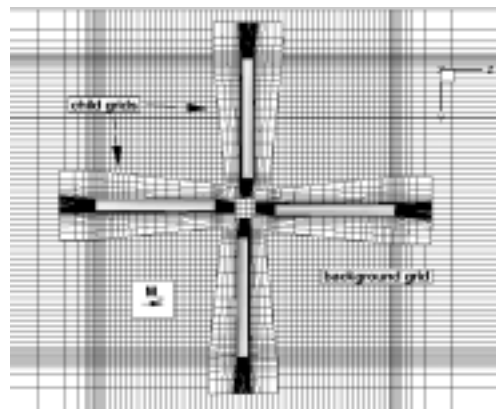
Figure 6   Top view of chimera grid system (7A rotor)

The grid dimensions are:

Table 1: Number of grid cells

	I	J	K	Cells on blade surface I	Cells on blade surface K	Total
Euler coarse	64	12	28	48	16	21 504
Euler medium	128	24	56	96	32	172 032
N-S medium	128	40	56	96	32	286 720
Chimera Child N-S	144	48	68	96	48	470 016
Chimera Background	64	144	144			1 327 104
Chimera total						3 207 168

The blade descretization for the S4 code consists of 20 blade elements with a reduced element size close to the blade tip. Further details on the blade discretization are given in Figure 7 and Table 1. The I-direction corresponds to the wrap-around direction, the J-direction to the direction normal to the blade surface and the K-direction to the radial direction. For the final validation computations with a refined grid in the vicinity of the blade have to be carried out.

6   Results

6.1   7A Rotor in High-Speed Forward Flight

The normal forces of the Euler computations without coupling are presented in Figure 8. The comparison

of the coarse grid (c) and the medium grid (m) results clearly shows that the coarse grid is not fine enough to resolve the 3d flow around the blade tip. The differences for radial positions r/R less than 0.9 between the results of the two grids are less pronounced. The two above observations indicate that the medium grid captures the main effects of the flow properly. Therefore all further computations were carried out with the medium grid.
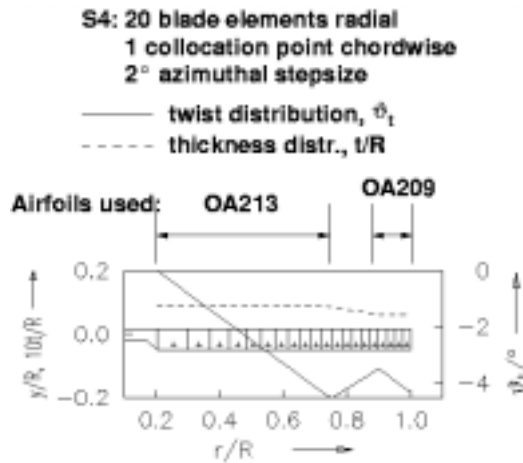
Figure 7 Blade discretization for S4
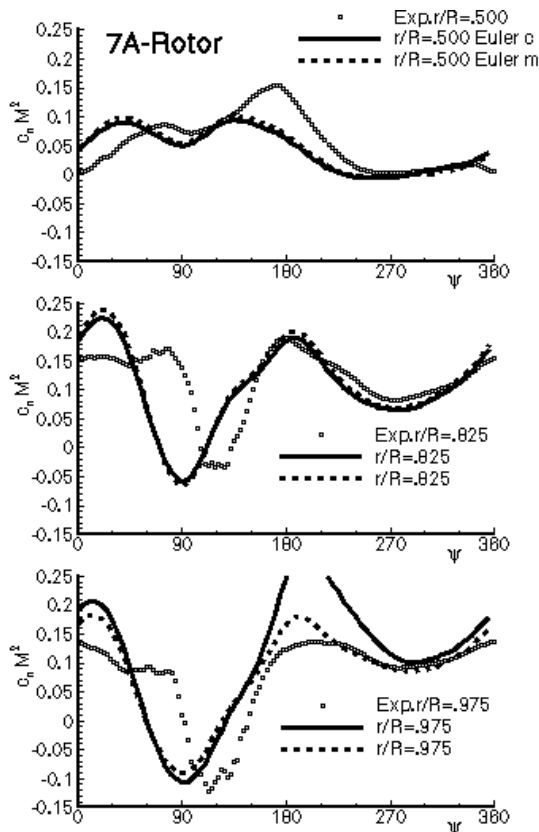
Figure 8 Normal forces distributions for the Euler computations without coupling (7A rotor)

Figure 9 shows the convergence of the control angles (θ_0, θ_S, θ_C) and the shaft angle α_q for the coupled 7A computations. The corresponding experimental values are given as square symbols. The computations were accepted as converged when the changes of the control angles and the shaft angle between two consecutive iterations was below 0.04°. All computations needed about 6 iterations to converge. The chimera computation was run for only 5 iterations. A fully converged chimera solution was not obtained for this paper.
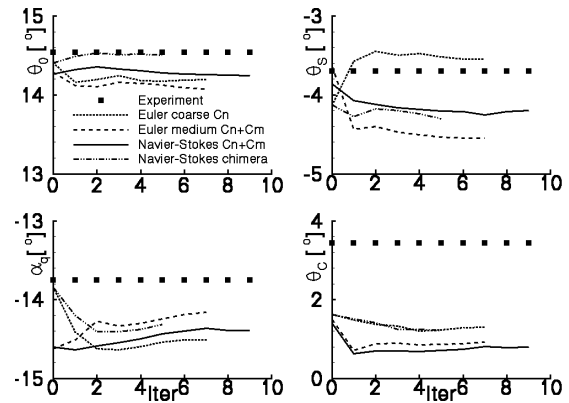
Figure 9 Convergence of control angles and shaft angle (7A rotor)
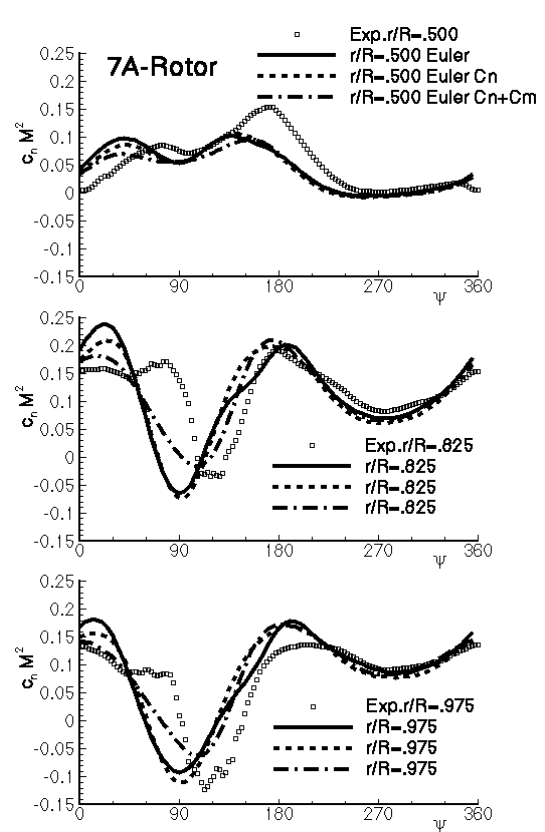
Figure 10 Normal force distributions for the coupled Euler computations (7A rotor)

The largest differences between the computed control angles/shaft angle and the measured ones of roughly 2° are observed for the lateral control angle θ_C. The shaft angle and the other control angles show differences of up to 0.7^o, which is a fair agreement.

The effect of a coupling with the normal forces and a coupling with both normal forces *and* moments assuming inviscid flow is presented in Figure 10 and Figure 11. The figures show that the coupling with the normal forces alone only slightly improves the agreement between the prediction and the experiment compared to the uncoupled computation. When the coupling is done for the normal forces *and* the pitching moment the negative peak of the normal forces is moved from 90° to 110° which is considerably closer to the negative normal forces peak in the experimental data.
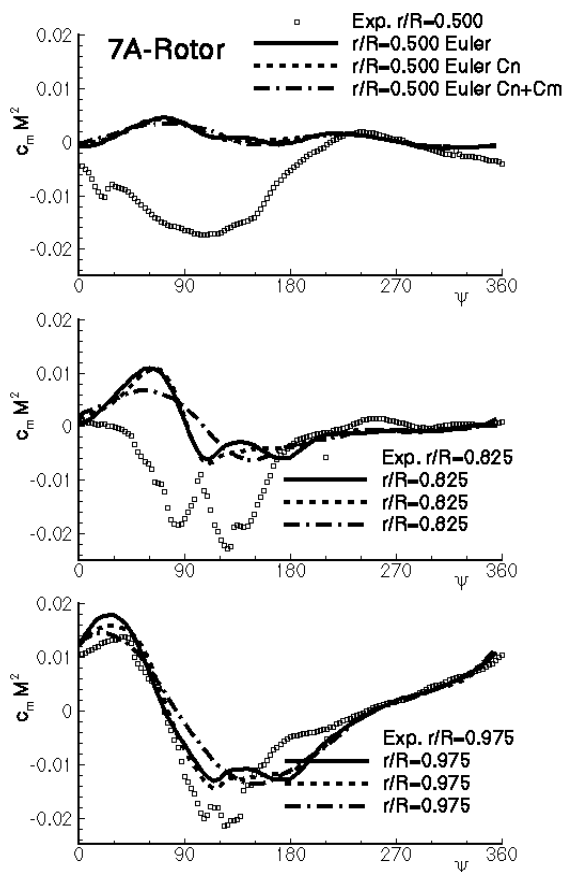
Figure 11 Moment distributions for the coupled Euler computations
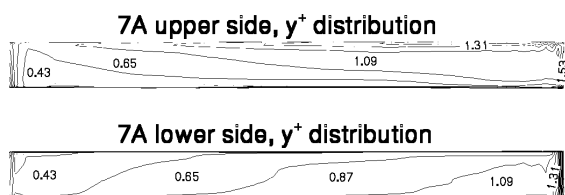
Figure 12 y+-distribution on the blade surface (7A rotor)
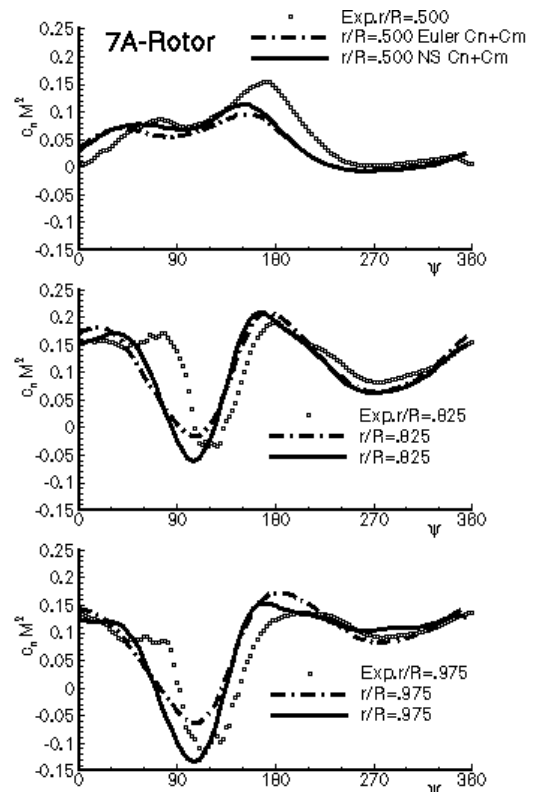
Figure 13 Normal force distributions of the coupled Euler and Navier-Stokes computations
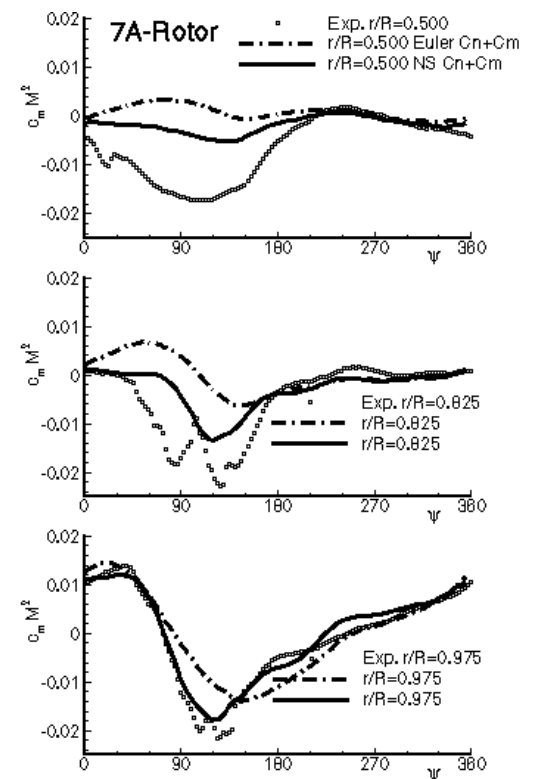
Figure 14 Moment distributions of the coupled Euler and Navier-Stokes isolated blade computations

27.6

For r/R=0.5 and r/R=0.825 it is striking that the Euler computation predicts a pitching moment which has the wrong sign for the first quarter of the revolution (see Figure 11), i.e. the predicted pitching moments are positive while the measured pitching moments are negative (-0.02). This is the reason why the negative normal forces peak is reduced when coupling is done with the Euler pitching moments (see Figure 10).
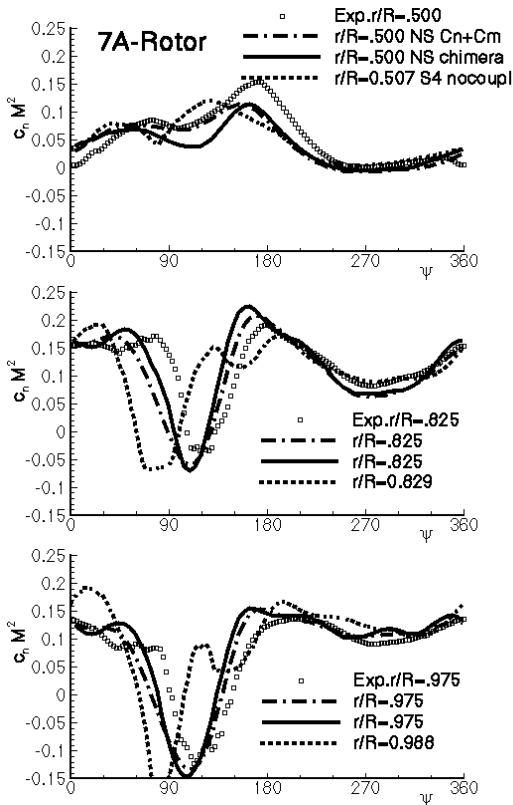
Figure 15 Normal force distributions of the coupled mono block, the chimera Navier-Stokes and the uncoupled S4 computations

Figure 12 shows the y^+-distribution of the first grid points normal to the wall for the 7A rotor. The most part of the blade has y^+-values which are around 1. At the very leading edge on the upper side y^+-values up to 2.5 are reached between r/R=0.7 and r/R=1.0. Only in the last row of cells at the very tip the y^+-values are between 2.5 and 3.5. This distribution of y^+-values is acceptable for resolving the high velocity gradients close to the blade surface. Still it should be kept in mind that this grid has only about 17 cells in the boundary layer which reproduces the main viscous effects but which cannot give a fully grid converged flow solution in the boundary layer. The flow was assumed to be fully turbulent.
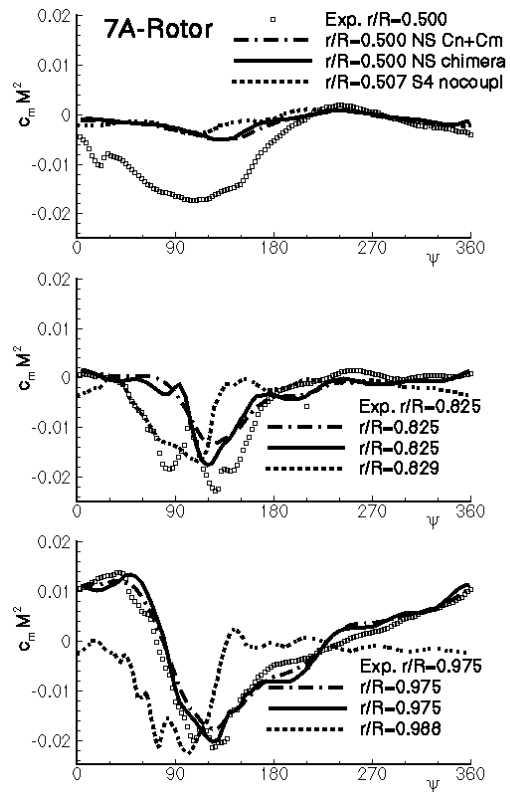
Figure 16 Moment distributions of the coupled mono block, the chimera Navier-Stokes and the uncoupled S4 computations
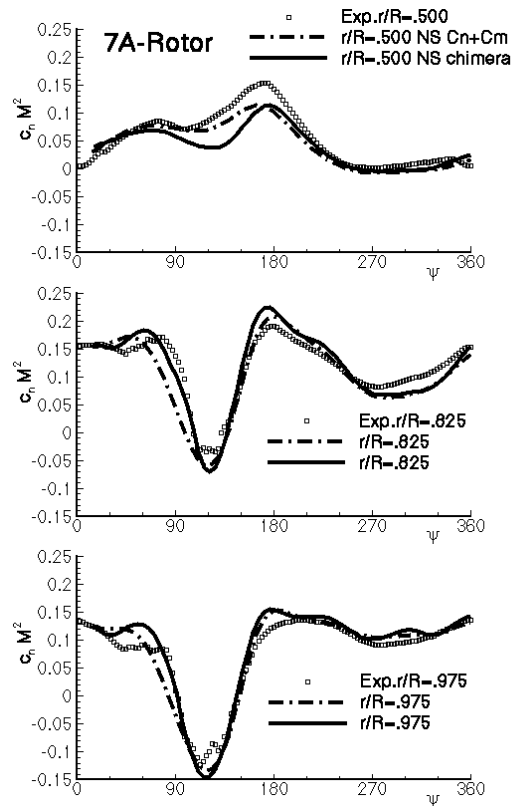
Figure 17 Shifted normal force distributions of the coupled 1 blade and the chimera N-S computations (7A rotor)

Figure 13 and Figure 14 compare the normal forces and moments computed based on the Euler and the Navier-Stokes equations with the measured data. The results of the Navier-Stokes computation agree considerably better with the experimental data. Especially the moments are better predicted (see Figure 14) which explains the improved agreement for the normal forces, because the coupling with the pitching moment directly influences the blade torsion which is of high importance for the blade aerodynamics. Figure 15 and Figure 16 compare the isolated blade Navier-Stokes computation with the chimera Navier-Stokes computation which was coupled with both normal forces and moments. In order to highlight the effect of the weak coupling the results of the S4-computation without coupling are given as a dashed line in Figure 15 and Figure 16. Comparing the uncoupled S4 results with the results of the coupled S4/FLOWer Navier-Stokes computation shows a clear improvement especially close to the blade tip for the normal forces as well as for the pitching moment.

line   CFD   grid, coupling
——— Euler coarse, C_n
······ Euler middle, C_n
- - - NS middle, C_n
— — Euler middle, $C_n + C_m$
— — NS middle $C_n + C_m$
— · NS/chimera $C_n + C_m$
□   Experiment
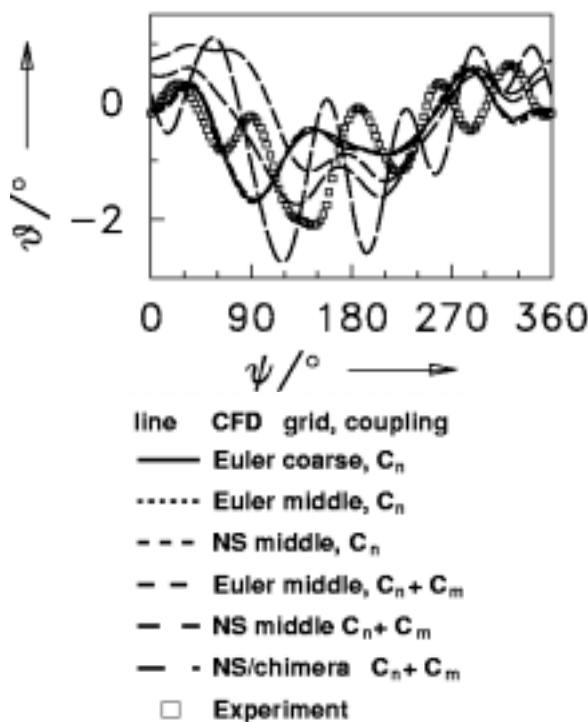
Figure 18 Elastic torsion at the blade tip (7A rotor)

In spite of the better physical model and of the enormous increase of the computational effort (see Table 2) the improvement because of the chimera technique compared to the isolated blade computation seems to be small. In order to ease the comparison of the isolated blade and the chimera computation Figure 17 shows the normal force distributions of the isolated blade shifted by +10 ° and the chimera

computation shifted by +12 ° azimuth. The chimera computation reproduces the overall shape of the normal forces considerably better than the isolated blade computation. The reason for the differences between the chimera and the isolated blade computation are the induced velocities of the wake which were neglected in the isolated blade computation.

The elastic torsion at the blade tip is plotted in Figure 18 for the different flow models (inviscid or viscous) and coupling procedures (with normal forces or with normal forces *and* moments). The best agreement between the computation and the measurement is obtained with the Navier-Stokes computation and a coupling with normal forces *and* moments (Cn+Cm). The 5/rev motion which is clearly seen in the experimental data is reproduced by the numerical method (Navier-Stokes computation with Cn+Cm coupling). The Navier-Stokes chimera computation coupled with normal forces and pitching moments overpredicts the elastic torsion at the blade tip after 5 coupling iterations, which shows that the 5/rev blade harmonics are stronger excited by the aerodynamic forces computed with the chimera method than those computed with the isolated blade. But it has to be kept in mind that the chimera results are not fully converged (see Figure 9).

6.2   7AD Rotor in High-Speed Forward Flight

For the 7AD rotor only isolated blade Navier-Stokes computations on the medium grid were carried out.
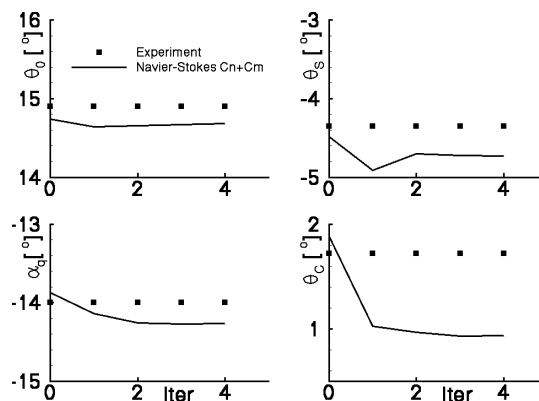
Figure 19 Convergence of control angles and shaft angle (7AD rotor)
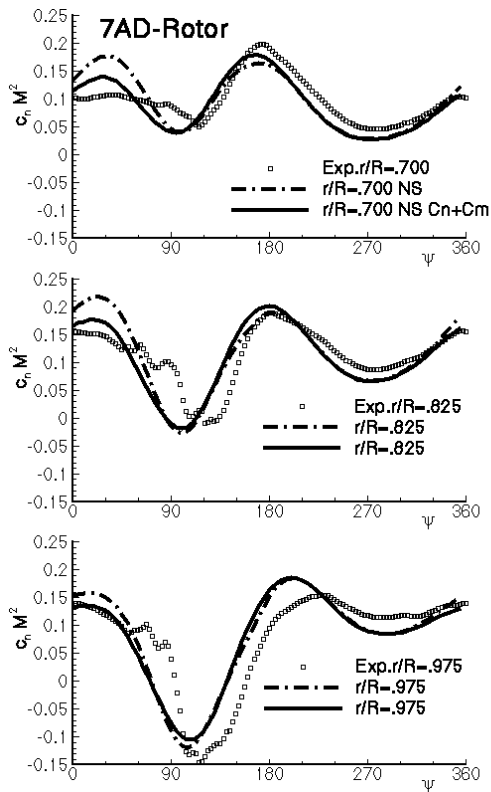
Figure 20 Normal force distributions of the uncoupled and the coupled single block Navier-Stokes computations (7AD rotor)

Figure 21 Moment distributions of the uncoupled and the coupled single block Navier-Stokes computations (7AD rotor)

The convergence of the weak coupling procedure is depicted in Figure 19. All computed control angles agree well with the experimental values. The lateral control angle shows the largest differences (0.7°) between computation and measurement. The coupling for the 7AD converges within 2 iterations which is considerably faster than for the 7A case. Figure 20 shows the normal force distributions for r/R=0.7, 0.825 and 0.975. The section at r/R=0.7 was chosen as the most inboard section because no experimental data was available for this test case at r/R=0.5. The overall agreement between predicted and measured normal forces in Figure 20 is good. The comparison of the normal forces for the uncoupled and the coupled Navier-Stokes computation for the 7AD rotor (Figure 20) shows smaller differences than the same comparison of the Euler computations for the 7A rotor (see Figure 10). The computed and measured pitching moments are compared in Figure 21. The agreement between prediction and measurement is similar to the results of the 7A rotor, although the differences close to the blade tip are larger.

The elastic blade torsion is given in Figure 22. The computed blade torsion does not show a 5/rev content in contrast to the results of the 7A rotor. The reason for this is not understood yet. The blade seems to be stiffer in this case than for the 7A test case which may be the reason for the extreme good convergence of the coupling procedure for the 7AD test case.
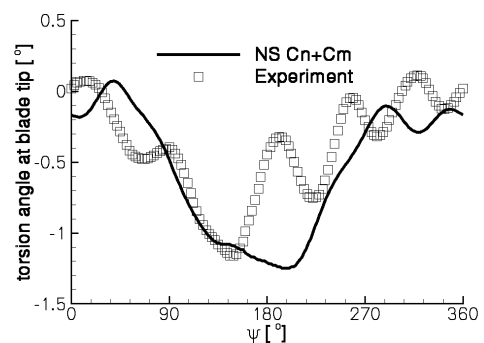
Figure 22 Elastic torsion at the blade tip (7AD rotor)

6.3 Sythesis of 7A and 7AD results

The weak coupling with normal forces *and* moments based on Navier-Stokes computations predicted the normal force distributions quite well except for a phase lag of about 10-15° azimuth. The predicted moments showed for both rotors considerable differ-

27.9

ences to the experimental data. The agreement of predicted and measured moments for the 7A rotor at r/R=0.975 was very good.

Table 2: Computational Effort

Description	Rotor	CPU-Time [h]/Rev on 1 Proc. NEC-SX5
Euler coarse	7A	0:14
Euler medium	7A	2:10
N-S	7A	3:30
N-S chimera	7A	49:15
N-S	7AD	3:30

The computational effort is given in Table 2. For this kind of application which includes deforming meshes and chimera functionalities a performance of only 1 GFLOPS is obtained on one processor of the DLR NEC-SX5. The reason for this poor performance is that the chimera search and most parts of the grid deformation tool in FLOWer 116.5 are not well vectorized. Activities to improve the situation have been started and the new modules will be tested soon.

The predicted and measured power consumption of the 7A and the 7AD rotor are presented in Figure 23. All power evaluations were done within the S4 code and only the coupling with isolated blade CFD computations was considered since no coupled chimera results were available for the 7AD rotor yet. The absolute power consumption is overpredicted by about 10%. The agreement on the absolute values is not improved by the weak coupling. When the prediction of the power difference between the two rotors is compared a considerable improvement because of the weak coupling can be observed. With the weak coupling a reduction in power consumption when comparing the 7AD and the 7A rotor of about 4% is predicted which compares fairly well to the measured 7% reduction.

7   Conclusion and Future Activities

A weak coupling procedure for coupling the rotor simulation code S4 and the Euler/Navier-Stokes solver FLOWer was presented. The method allows to produce trimmed CFD solutions for rotors in high speed forward flight accounting for elastic blade deformations and viscous effects. The weak coupling procedure was applied to high-speed forward flight test cases of the 7A and the 7AD rotor. Isolated blade computations were carried out for both rotors while a chimera computation around the whole 4-bladed rotor was carried out only for the 7A rotor. The predicted pitching moment computed with the assumption of inviscid flow (Euler) showed large differences compared to the experimental data. Between 0° and 90° azimuth the Euler pitching moment even had the wrong sign. A clear improvement of the

solution with respect to the existing experimental data because of the weak coupling was proven.
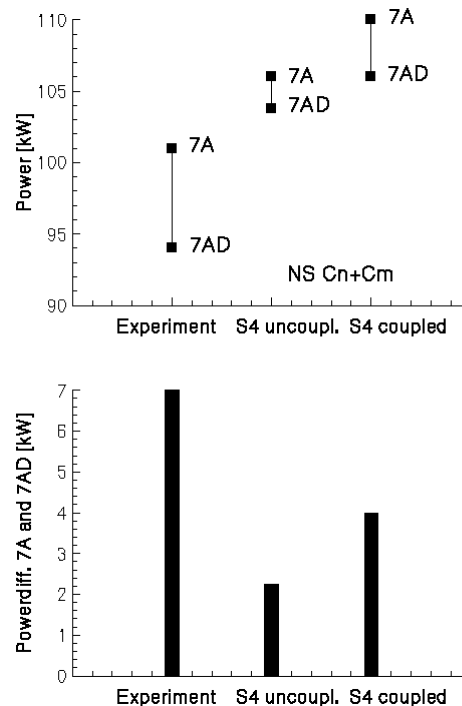
Figure 23   Power for 7A and 7AD rotor and power difference between these rotors

The well known negative peak in the normal forces distribution close to the blade tip around 90°-120° for elastic blades in high speed forward flight was well reproduced with the coupled Navier-Stokes computation although the computational results show a phase shift of about 10-15° azimuth. While the predicted elastic torsion for the 7A test case showed a considerable content of a 5/rev motion this was not the case for the 7AD rotor. The reason for this unexpected difference has to be clarified. The chimera technique provided more accurate results at the cost of an increase of computational effort by more than one order of magnitude.

Although the method was based on isolated blade computations it was able to predict the performance differences between the 7A and the 7AD rotor in high-speed forward flight fairly well while the absolute power was overpredicted for both rotors by about 10%.

The next steps will be to carry out chimera computations for the 7AD rotor and to compare the performance prediction based on chimera computations. Then the method will be applied to other flight conditions. Furthermore the coupling procedure will be extended to include the tangential forces. This will have an important effect on the prediction of the power consumption and should improve the accuracy of the power prediction. In this context a procedure

has to be developed which allows to account for the laminar/turbulent transition. In addition the lead-lag motion has to be taken into account which may explain the phase differences between the computations and the measurements. Furthermore the coupling will also be done with the Eurocopter standard tool HOST.

For an industrial application the user workload has to be considerably reduced by automatization of the coupling procedure. Finally the accuracy and efficiency of the weak coupling approach has to be assessed in comparison to the strong coupling approach. This comparison will be carried out in the CHANCE project together with ONERA and the University of Stuttgart.

8   References

[1] Pahlke, K. and Chelli, E.: „Calculation of Multibladed Rotors in Forward Flight Using a 3D Navier-Stokes Method", 26th ERF, The Hague, The Netherlands, 26-29 September 2000.

[2] Servera, G.; Beaumier, P. and Costes, M.: „A Weak Coupling Method Between the Dynamics Code Host and the 3D Unsteady Euler Code Waves", 26th ERF, The Hague, The Netherlands, 26-29 September 2000.

[3] Sidès, J.; Pahlke, K. and Costes, M.: „Numerical Simulation of Flows around Helicopters", First ONERA-DLR Aerospace Symposium, Paris, 21-24 June 1999, to appear in Aerospace Science and Technology.

[4] Pahlke, K.; Sidès, J. and Costes, M.: „Towards the CFD Computation of the Complete Helicopter: First Results Obtained by French and German Research Centers", Second ONERA-DLR Aerospace Symposium, Berlin, 15-16 June 2000, to appear in Aerospace Science and Technology.

[5] Pahlke,K.: "Berechnung von Strömungsfeldern um Hubschrauberrotoren im Vorwärtsflug durch die Lösung der Euler-Gleichungen", DLR-Forschungsbericht 1999-22, ISSN 1434-8454, 1999

[6] Kroll, N.; Rossow, C.C.; Becker, K. and Thiele, F.: "MEGAFLOW-A Numerical Flow Simulation system", ICAS-congress, September 1998, Melbourne, Australia

[7] Jameson, A.; Schmidt, W. and Turkel, E.: "Numerical Solutions of the Euler Equations by Finite Volume Methods Using Runge-Kutta Time-Stepping Schemes", AIAA Paper 81-1259, 1981

[8] Baldwin, B. and Lomax, H., "Thin Layer Approximation and Algebraic Model For Separated Turbulent Flows", AIAA-Paper 78-0257,197

[9] Degani and Schiff, L., "Computation of Turbulent Supersonic Flows around Pointed Bodies having Crossflow Separation", Journal of Computational Physics Vol. 66, pp. 176-196, 1986.

[10] Jameson, A.: „Time Dependent Calculation Using Multigrid, with Applications to Unsteady Flows Past Airfoils and Wings", AIAA Paper 91-1596, 1991.

[11] Gaitonde, A. L. and Fiddes, S.: „A Three-Dimensional Moving Mesh Method for the Calculation of Unsteady Transonic Flows", University of Bri-

stol, Rep. No. 483, Sept. 1993.

[12] O. Brodersen,O.; M. Hepperle, M.; Ronzheimer, A.; Rossow, C.-C. and Schöning, B.: „The Parametric Grid Generation System MegaCads", Proc. of 5th International Conference on Numerical Grid Generation in Computational Field Simulation, Ed. B.K. Soni et.al., 1996, 353—362.

[13] Brodersen, O.; Ronzheimer, A.; Ziegler, R.; Kunert, T.; Wild, J. and Hepperle, M.: „Aerodynamic Applications using MegaCads", Proc. of 6th International Conference on Numerical Grid Generation in Computational Field Simulation, Editor M. Cross et.al., 1998, 793—802.

[14] van der Wall, B. G.: "An Analytical Model of Unsteady Profile Aerodynamics and its Application to a Rotor Simulation Program", 15th European Rotorcraft Forum, Amsterdam, Netherlands, 1989.,

[15] van der Wall, B. G.: "Analytic Formulation of Unsteady Profile Aerodynamics and its Application to Simulation of Rotors", DLR-FB 90-28, 1990, also: ESA-Report No. ESA-TT-1244, 1992.

[16] Beaumier, P.; Prieur, J.; Rahier, G.; Spiegel, P.; Demargne, A.; Tung, C.; Gallmann, J.M.; Yu, Y.; Kube, R.; van der Wall, B.G.; Schultz, K.J.; Splettstoesser, W.R.; Brooks, T.F.; Burley, C.L.; Boyd, D.D.: "Effect of Higher Harmonic Control on Helicopter Rotor Blade-Vortex Interaction Noise: Prediction and Initial Validation", AGARD-CP-552, 1995; also: 75th Fluid Dynamics Symposium, Berlin, Germany, 1994

[17] Petot, D.; Arnaud, G.; Harrison, R.; Stevens, J.; Teves, D.; van der Wall, B.G.; Young, C. and Széchényi, E.: "Stall Effects and Blade Torsion - an Evaluation of Predictive Tools", 23rd European Rotorcraft Forum, Dresden, Germany, 1997.

[18] Leiss, U.: "A Consistent Mathematical Model to Simulate Steady and Unsteady Rotor-Blade Aerodynamics", 10th European Rotorcraft Forum, Den Haag, Netherlands, 1984.

[19] Leiss,U.: "Unsteady Sweep - A key to Simulation of Threedimensional Rotor Blade Airloads", 11th European Rotorcraft Forum, London, England, 1985.

[20] van der Wall, B.G. and Leishman, J.G.: "On the Influence of Time-Varying Flow Velocity on Unsteady Aerodynamics", Journal of the American Helicopter Society, Vol. 39, Nr. 4, 1994.

[21] van der Wall, B.G.: "Simulation of HHC on Helicopter Rotor BVI Noise Emission using a Prescribed Wake Method", 26th European Rotorcraft Forum, The Hague, Netherlands, 2000.

[22] Goepel, C. and van der Wall, B.G.: "Berechnung der induzierten Geschwindigkeiten des Rotorversuchsstandes ROTEST im DNW", DLR IB 111-89/27, 1989.

[23] Beaumier, P.; Costes, M. and Gavériaux, R.: "Comparison Between FP3D full Potential Calculations and S1 Modane Wind Tunnel Test Results on Advanced Fully Instrumented Rotors" 19th ERF, Cernobbio, Como (Italy), Sept. 1993.

27.11